Letter

Water structures and anisotropic dynamics at Pt(211)/water interface revealed by machine learning molecular dynamics

Fei-Teng Wang[1], Xiandong Liu[2,3,*] and Jun Cheng[1,4,5,*]

[1] State Key Laboratory of Physical Chemistry of Solid Surfaces, iChEM, College of Chemistry and Chemical Engineering, Xiamen University, Xiamen 361005, People's Republic of China
[2] State Key Laboratory for Mineral Deposits Research, School of Earth Sciences and Engineering, Nanjing University, Nanjing, Jiangsu 210023, People's Republic of China
[3] Frontiers Science Center for Critical Earth Material Cycling, Nanjing University, Nanjing, Jiangsu 210023, People's Republic of China
[4] Laboratory of AI for Electrochemistry (AI4EC), IKKEM, Xiamen 361005, People's Republic of China
[5] Institute of Artificial Intelligence, Xiamen University, Xiamen 361005, People's Republic of China

E-mail: xiandongliu@nju.edu.cn and chengjun@xmu.edu.cn

CrossMark

Abstract

Water molecules at solid–liquid interfaces play a pivotal role in governing interfacial phenomena that underpin electrochemical and catalytic processes. The organization and behavior of these interfacial water molecules can significantly influence the solvation of ions, the adsorption of reactants, and the kinetics of electrochemical reactions. The stepped structure of Pt surfaces can alter the properties of the interfacial water, thereby modulating the interfacial environment and the resulting surface reactivity. Revealing the *in situ* details of water structures at these stepped Pt/water interfaces is crucial for understanding the fundamental mechanisms that drive diverse applications in energy conversion and material science. In this work, we have developed a machine learning potential for the Pt(211)/water interface and performed machine learning molecular dynamics simulations. Our findings reveal distinct types of chemisorbed and physisorbed water molecules within the adsorbed layer. Importantly, we identified three unique water pairs that were not observed in the basal plane/water interfaces, which may serve as key precursors for water dissociation. These interfacial water structures contribute to the anisotropic dynamics of the adsorbed water layer. Our study provides molecular-level insights into the anisotropic nature of water behavior at stepped Pt/water interfaces, which can influence the reorientation and distribution of intermediates, molecules, and ions—crucial aspects for understanding electrochemical and catalytic processes.

---

* Authors to whom any correspondence should be addressed.

1

1. Introduction

Solid/liquid interfaces are ubiquitous in natural and engineered systems [1], playing a crucial role in geochemistry [2], electrochemistry [3], and corrosion [4]. The molecular structures at these interfaces [5] exhibit complex interactions between water molecules, ions, and solid surfaces [6–9], creating a heterogeneous environment with features like hydration layers [10], adsorption sites [11], and varying ion distributions [12]. The dynamics at these interfaces are also complex, driven by both structural organization and thermal fluctuations [13], leading to constant movement and reorganization at different spatial and temporal scales. Understanding and controlling interfacial processes requires detailed characterization of the interface structure and dynamics [4, 14–17].

The structure and dynamics of water molecules at solid/liquid interfaces can significantly influence the overall interfacial processes. Studies have shown that water molecules can exhibit different structural arrangements and hydrogen-bonding patterns compared to bulk water [18–25]. These unique water structures may play an important role in governing various interfacial phenomena, such as ion adsorption, charge transfer, and even chemical reactions [26, 27]. However, the precise water structures at specific solid/liquid interfaces that contribute to these processes are not fully understood. For example, surface x-ray diffraction and near-edge x-ray adsorption fine structure measurements showed two distinct O sites above the step Pt atoms of Pt(211), supporting that water is stabilized by forming 1D zigzag water chains [22, 28]. Nevertheless, calculation suggested that simple 1D chains at the step edge are not thermodynamically stable when the coverage is increased [18]. A recent study showed that the chain structure at Pt(211) disappears as water adsorption saturates the surface to form an incommensurate, disordered network of water rings of different size [24]. At ambient conditions, when metal interfaces are in contact with liquid water, the molecular structure of the interface is no longer directly accessible as it is at monolayer coverages and ultrahigh vacuum conditions [1]. Spectroscopic techniques have faced challenges in unambiguously identifying these complex water structures due to difficulties in spectral deconvolution [29–32]. Developing accurate computational models that capture the intricate interplay between water, ions, and the solid surface is crucial for improving our understanding of these interfacial processes [33, 34]. Explicit interface models that include the adsorbed water layer and surrounding water molecules, along with accurate descriptions of metal-water and water-water interactions, can provide the necessary structural and dynamic information. *Ab initio* molecular dynamics (AIMD) is a powerful tool for this purpose, although its high computational cost presents a challenge [35].

In this study, we have developed a machine learning potential (MLP) to investigate the atomic-scale structure and dynamics of water molecules at the Pt(211)/water interface. Our findings revealed the presence of distinct types of water molecules with unique angular distributions and pair configurations within the adsorbed layer. These water structures, which are strongly influenced by the anisotropic nature of the stepped Pt(211) surface, lead to pronounced anisotropies in the water dynamics, primarily attributed to the directionality of hydrogen bonding interactions. Specifically, we observed that water molecules in direct contact with the Pt(211) surface exhibit preferred orientations and enhanced residence times compared to bulk-like water molecules. Additionally, the stepped geometry of the interface promotes the formation of well-defined water pair structures, which exhibit characteristic lifetimes and diffusion characteristics. These insights into the structure and dynamics of the water layer at the Pt(211)/water interface have important implications for understanding a wide range of interfacial phenomena, including water dissociation and ions solvation at stepped Pt/water interfaces.

2. Method

Models and computations

The Pt(211)/water interface is modeled using orthogonal $6 \times 6 \times 6$ Pt slabs with water molecules filled in between the top and bottom of the Pt surfaces. The lattice parameter for the supercell is 16.869,13.774 and 40.00 Å along $x/y/z$ direction. Here, the water density has been determined to be 0.97 g cm^{-3} at the middle 7 Å for Pt(211)/water interface. For the production run, we expand the both the models to orthogonal $12 \times 12 \times 6$ Pt slabs. All the density functional theory (DFT) calculations are performed in CP2K/Quickstep [36]. The Goedecker–Teter–Hutter (GTH) pseudopotentials [37, 38] are used to describe the atoms: the H is described by GTH-PBE-q1, with all electrons in the valence, O atom is described by the GTH-PBE-q6 with 2 s and 2p electrons in the valence, and Pt is described by the Pt GTH-PBE-q10 with 5d and 6 s electrons in the valence. The DZVP-MOLOPT-SR-GTH Gaussian basis [39] set is used to all atom types except for Pt, which uses a developed basis set for the GTH-PBE-q10 of Pt by Le *et al* [40]. The cutoff of the plane wave energy is set to 1000 Ry. The Perdew–Burke–Ernzerhof (PBE) functional is utilized to describe the exchange-correlation effect [41]. Grimme D3 correction is included to consider the dispersion interaction [42].

MLP and MD simulations

We utilize the DPGEN workflow to iteratively update the training dataset for developing MLPs. This workflow consists of

three main parts: training, exploration, and labeling. Detailed descriptions can be found in the original literatures [43, 44]. Utilizing this workflow, we have updated the dataset of interfacial structures to 4280 for Pt(211)/water. To conduct MD simulation with first principles accuracy and high efficiency, we use the Deep Potential model to learn the structure-dependent energies and forces. The se_a descriptor is used in this work [44]. The training process contains two sets of deep neural networks: the embedding network for training descriptors and the fitting network for training MLPs. The size of embedding networks is set to (25, 50, 100) and the fitting network is set to (240, 240, 240). The cutoff radius of descriptors is set to 8.0 Åand the weight decays smoothly from 0.5 to 8.0 Å. For the active learning process, 200 000 steps are used to train the potential. For the final production of MLPs, 2000 000 steps are used.

The molecular dynamics (MD) simulations are performed with both large-scale atomic/molecular massively parallel simulator (LAMMPS) package [45] and CP2K package [36]. For the exploration in the DPGEN, we use LAMMPS to conduct MD. The simulation is conducted in NVT ensemble and we set the temperature to 330/430/530 K to include the configurations distributed around these temperatures. The time step is set to 0.5 fs and Nose–Hoover thermostat is used to control temperature with temperature damping parameter setting to 100 fs [46, 47]. For the equilibration and production run, we used the CP2K package. For the convenience of comparison to previous AIMD simulations [48], we performed the second generation Car–Parrinello MD in canonical ensemble (NVT) using a timestep of 0.5 fs. The Langevin friction coefficient γ_D is set equal to $0.001\ fs^{-1}$. The intrinsic friction coefficients γ_L are set to $2.2 \times 10^{-4}\ \text{fs}^{-1}$ for H_2O and $5 \times 10^{-5}\ \text{fs}^{-1}$ for Pt. For all the validation runs, 1 ns simulation is conducted.

3. Results

The Pt(211) surface has (111) terraces separated by (100) steps (figure 1(a)). Our model includes 216 Pt atoms and 190 water molecules, accurately representing the interface and bulk water. The water density in the central region is 0.97 gcm^{-3}. [48] (more details in the supplementary). We trained a MLP for this system using an active learning workflow [43]. (This workflow began with 200 structures from a previous simulation [48]. Further details can be found in the supplementary.) This MLP accurately predicts energy and force (table S1). We then added k-point correction to ensure converged energy/force over k-point densities (figure S1). The root mean square error of energy and force between first principles calculation and MLP prediction are below 0.6 meV/atom and 80 meVÅ^{-1} (table S1), respectively. Finally, we performed machine learning molecular dynamics (MLMD) simulations using the trained MLP and an expanded 2 × 2 × 1 model (figure S2). These simulations showed no significant energy drift over 10 ns, with an average temperature of 392 K (figure S3).

We compared oxygen density profiles obtained from both MLMD and AIMD simulations (figure 1(b)) [48]. Using the

average z-position of the step Pt atoms as the reference plane, we found consistent profiles between MLMD and previous AIMD simulations. This consistency indicates that the MLMD model accurately captures the structural features of the water layer at the stepped Pt interface. Based on the vertical distances of the oxygen density (table S2), we classified the water molecules into four categories: A, B, V, and C. Water molecules within the middle five Åregion were defined as bulk water and labeled as L. Unlike the behavior observed on the basal plane, [49] where water A was solely attributed to chemisorbed water molecules, this region now also contains physisorbed water molecules (figure S4). Analysis of the angle probability distribution (figure 1(c)) revealed a population of water molecules with the OH vector pointing toward the surface at $z < 2.65$ Å. These molecules are not chemisorbed on top of the stepped Pt atoms but are physisorbed above the terrace Pt atoms. They are stabilized by hydrogen bond interactions with chemisorbed water molecules. However, further decomposition of water A into more fundamental components solely based on z-coordinate and the probability distribution of $\cos\theta$ will be difficult.

To address this challenge, we used the joint probability distribution of both OH vector angles relative to the surface normal. This analysis, shown in figure 2(a), allowed us to further subdivide water A into three distinct regions (A^I, A^{II}, A^{III}). Table 1 outlines the criteria for classifying water A and B into these distinct regions (figure 2(b)). Coverage analysis revealed that the probability of A^{III} is significantly lower compared to the other regions. The step density of chemisorbed water molecules A^I is 0.596 (approximately 0.20 relative to the surface Pt atoms), consistent with previous AIMD simulations [48]. The overall surface coverage of A+B is approximately 0.70. In the following section, we will delve into the orientation and arrangement of the prominent water pairs and explore their influence on water dynamics.

To provide a more precise orientation description of these distinct water molecules, we analyzed the directionality of the oxygen–hydrogen vector (figure 2(c)). We defined a vector pointing from the oxygen atom (O) to the hydrogen atom (H) and projected this vector onto the plane perpendicular to the surface normal. The angle between this projected vector and the vector along the step is denoted as θ'. Figure 2(d) depicts the water structures, while figures 2(e)–(j) illustrate the probability distribution of the projected angle at various O–H distances. Figure 2(e) shows the probability distribution for A^I, which primarily adsorbs on top of the stepped Pt atoms (figure S5). For O–H distances less than 0.95 Å, there is a negligible probability distribution, indicating the absence of hydrogen bond formation on top of A^I. When the O–H distance is approximately 1.70 Å, the probability distribution along the step (dcosθ) is symmetric, while it is asymmetric perpendicular to the step (dsinθ). Further analysis (figure S6) reveals that when water A^I acts as a hydrogen acceptor, it primarily accepts hydrogen along the step. Conversely, as a hydrogen donor, it exhibits a preferred orientation perpendicular to the step, with θ' mainly concentrated at $0° \pm 45°$. Figure 2(f) shows the angle distribution of A^{II}. Our previous study showed that A^{II} at the basal plane/water
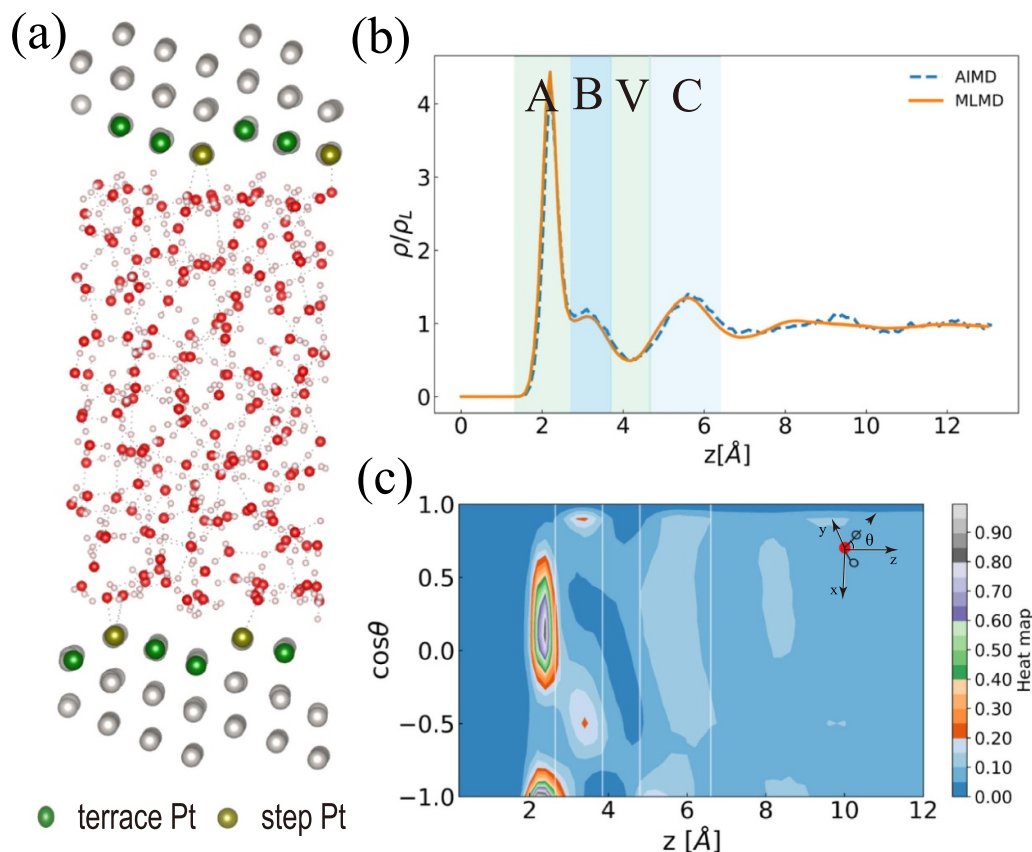
Figure 1. The model and structural feature of Pt(211)/water interface. (a), The Pt(211)/water model. (b), The oxygen density profile along the surface normal obtained from AIMD and MLMD. Here, the average z value of step Pt atoms are chosen as the reference plane. (c), The probability distribution of $\cos\theta$, where θ is defined as the angle between OH vector and the surface normal.

interface primarily resides in the second adsorbed layer (the physisorbed layer). However, at the Pt(211)/water interface, the recesses (terrace rows) formed by the stepped platinum surface provide space for water molecules to move downward. This allows physisorbed water molecules to enter the chemisorbed peak region in the z-direction when considering the plane of the step Pt atoms as the reference. As a hydrogen donor (figure S6), A^{II} contributes hydrogen only along the step direction. As a hydrogen acceptor, it primarily accepts hydrogen perpendicular to the step. This indicates that the plane of A^{II} is parallel to the step rows. Although the coverage of A^{III} (figure 2(g)) is low, we find that it also contributes hydrogen perpendicular to the step with a preferred orientation similar to A^I. Water B exhibits a distinctive asymmetric hydrogen bond orientation perpendicular to the step, with a preferred orientation of θ' at $180° \pm 45°$. This preference complements that of water A. B^I (figure 2(h)) primarily resides on top of the terrace Pt atoms (figure S5). The joint probability distribution (figures 2(a) and (b)) shows that A^{III} and B^I have similar angle distributions. However, as donor water molecules (figure S7), A^{III} and B^I exhibit opposite orientation preferences perpendicular to the step. For B^{II}, hydrogen bonding along the step direction is rare. The orientation preference applies to both donor and acceptor water molecules (figure S7), suggesting that the plane of B^{II} may be perpendicular to the step. B^{III} exhibits an

Table 1. The classification of adsorbed water molecules. Here z is defined as the distance of oxygen atoms to the reference plane (the average z values of stepped Pt). The coverage is calculated as the number of water molecules/the number of surface Pt atoms.

	z[Å]	$\cos\theta_1$, $\cos\theta_2$	Coverage
A^I	1.60–2.65	$[-0.50, 0.70]$ and $[-0.50, 0.70]$	0.20 ± 0.02
A^{II}	1.60–2.65	$[-1.00, -0.50]$ or $[-1.00, -0.50]$	0.26 ± 0.02
A^{III}	1.60–2.65	$[0.70, 1.00]$) or $[0.70, 1.00]$	0.01 ± 0.01
B^I	2.65–3.70	$[0.60, 1.00]$ or $[0.60, 1.00]$	0.06 ± 0.02
B^{II}	2.65–3.70	$[-1.00, 0.00]$ and $[-1.00, 0.00]$	0.02 ± 0.01
B^{III}	2.65–3.70	$([0.00, 0.60]$ and $[-1.00, 0.60])$ or $([-1.00, 0.60]$ and $[0.00, 0.60]$)	0.15 ± 0.02

angle distribution resembling that of A^{II}, but with a more flexible water orientation.

These water molecules form the prominent building blocks of the hydrogen bond network. When an intermediate replaces the chemisorbed A^I, its orientation will be modulated by the surrounding water molecules, affecting their thermodynamics and kinetics.

To better understand the water pairs potentially influencing water dissociation and other local solvent structures, we examined the radial distribution functions (RDFs) of
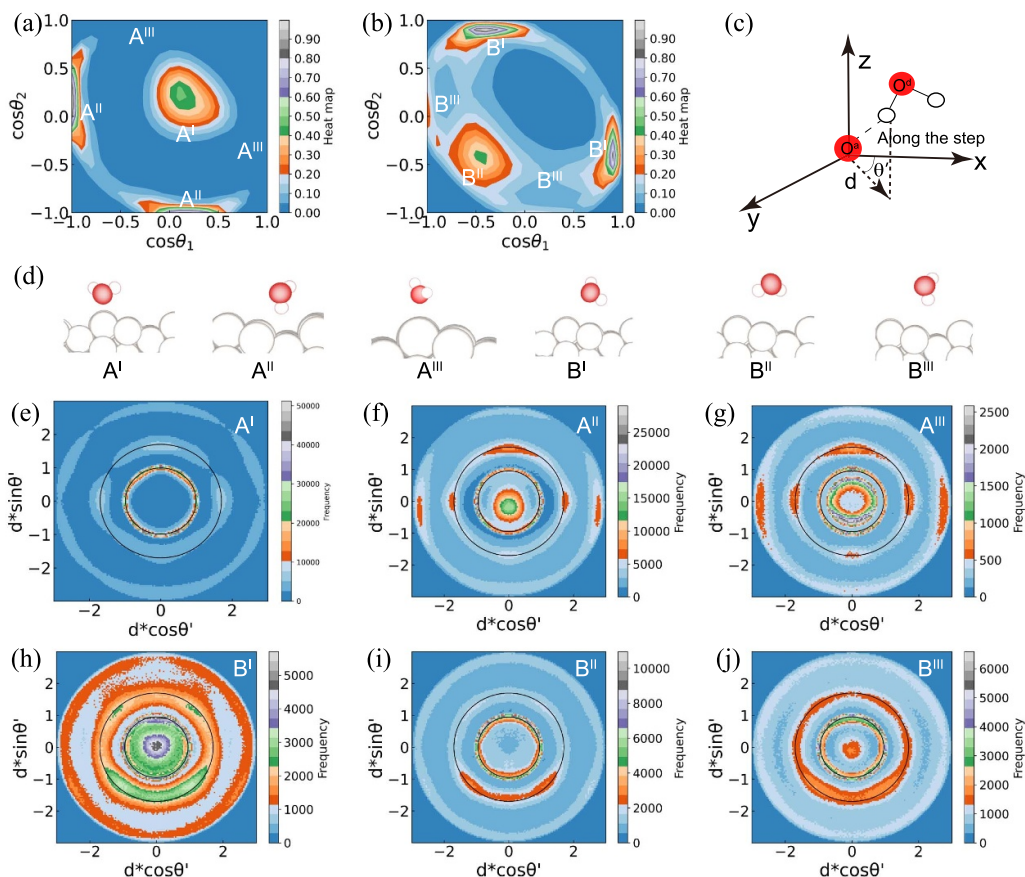
Figure 2. The orientation of the hydrogen bonds of different type of water molecules. (a), The joint probability distribution of water molecules in A region. Here θ_1 and θ_2 correspond to the angle between the two OH vectors of a water molecule and the surface normal. (b), The same distribution as A but for water molecules in B region. (c), Schematic illustration of the projection of O–H vector to the reference plane. Here, d is the distance between oxygen and hydrogen. θ' corresponds to the angle between OH vector and the vector along the step rows. The O–H can be the covalent bond or the hydrogen bond. (d), The representative adsorbed water structures. (e)–(j), The density distribution of the OH distance at different angles for A^I, A^{II}, A^{III}, B^I, B^{II}, and B^{III}.

the adsorbed water molecules. Each type of water molecule (as defined in the previous section) was used as a reference atom. The results (figures 3(a) and (c)) highlight prominent water pairs between A^I and A^{II}, A^I and B^I, as well as A^{II} and A^{II}. In the A^I-A^{II} pair, A^I sits atop the stepped Pt atoms, while A^{II} resides on top of the terrace Pt atoms. A^I donates its hydrogen to A^{II}, which accepts hydrogen with its water plane parallel to the step rows. The O–H vector orientation preferences of A^I and A^{II} suggest that A^{II} primarily resides above terrace atoms close to the lower (100) step atoms (figure S5). In the A^I and B^I pair, A^I also donates hydrogen to B^I. Considering the coverage of A^I, A^{II}, and B^I, we know that this type of hydrogen bond is secondary to A^I but prominent for B^I. For this pair, B^I resides above terrace atoms close to the upper (100) step atoms. For the A^{II} and A^{II} pair, these water molecules primarily reside above terrace atoms and form hydrogen bonds parallel to the step rows. Previous analysis indicates that these water molecules have planes parallel to the step rows. Compared to the prominent water pairs, interactions between A^I-A^I, A^I-A^{III}, A^I-B^{II}, A^I-B^{III}, A^{II}-A^{III}, and A^{II} with water B are less abundant. Interactions within water B molecules are further decreased (figure 3(c)). However, these

less abundant pairs are necessary components of the overall hydrogen bond network, which may be overlooked in low-water-coverage vacuum models.

To support this point, we extracted the *z*-coordinates of oxygen atoms within 3 Å of the referenced oxygen atoms of the adsorbed water molecules (figure S8). Most oxygen atoms interacting with A^I and A^{II} are chemisorbed and physisorbed water molecules. For A^{III}, a small fraction of interacting water molecules reside in the V region. Physisorbed water molecules in the B region primarily interact with the chemisorbed water molecule A, but they also have connections to water molecules in the C region (figure 3(d)). This suggests that adsorbed water molecules are not isolated from non-adsorbed water molecules, but they mainly interact through water molecules in the B region. In figures 3(a) and (d), a vertical line is drawn at $r = 2.6$ Å for reference, which corresponds to the shortest peak position of the water pairs (exactly between A^I and B^{III}). Pairs containing A^I exhibit a peak position close to this line. However, for physisorbed water molecules and VC, the peak positions are slightly larger. These differences suggest that these water pairs may play different roles in the water dissociation process.
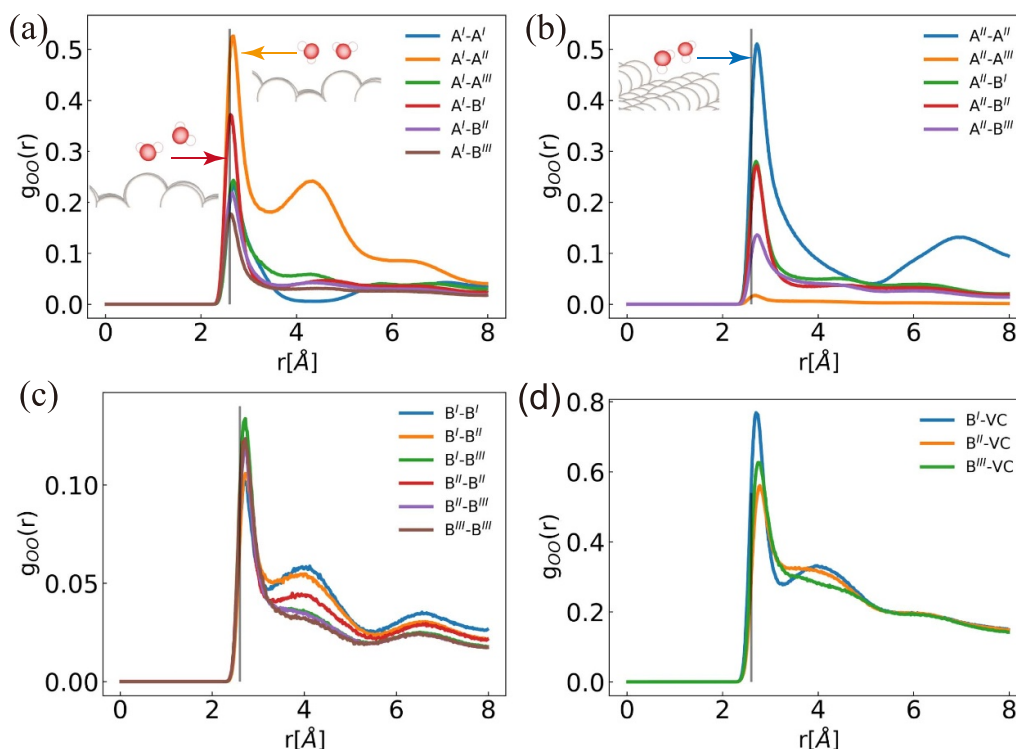
Figure 3. The water pairs analysis. (a)–(d), The radial distributions functions of oxygen-oxygen of different types of water molecules. The legend shows the referenced oxygen atoms (the first label) and the observed oxygen atoms (the second label). The inset figures in (a) and (b) show the prominent water pairs.

After identifying the prominent water pairs, we investigated their role in interfacial water dynamics. Using the mean squared displacement method, we tracked displacement every 10 ps over 3 ns and then calculated diffusion coefficients. Since A^I is chemisorbed on top of the step Pt atoms, it was excluded from the diffusion dynamics study. Due to the low coverage of A^{III} and the exchange of different types of water B molecules during the observation period (figure S12), we focused on studying the diffusion dynamics of A^{II}, B, V, C, and L.

We analyzed the one-dimensional diffusion of water molecules along and perpendicular to the step rows. A^{II} exhibits anisotropic diffusion dynamics with higher diffusion coefficients along the step (figure 4(a)). This observation aligns with the definition of A^{II}, which shares a similar z-values with A^I. This environment restricts the movement of A^{II} perpendicular to the step, resulting in lower diffusion coefficients in this direction. Additionally, figure 2(d) shows the absence of hydrogen bonds on top of A^I, indicating limited facilitation of water molecule transfer in the B region perpendicular to the step. While this hindrance is less severe for B compared to A^{II}, anisotropic water diffusion dynamics are still observed in the B region. As water molecules move further away from the interface, the anisotropic water diffusion dynamics become isotropic. This is consistent with the observation of isotropic hydrogen bond orientation distribution in bulk water L (figure S10). Aside from the directionality of the diffusion dynamics, it can also be observed that the diffusion will become slow

from bulk water to the interfacial water molecules. The diffusion coefficient of bulk water molecules is also consistent with the results of our recent study.

Slower interfacial water diffusion dynamics generally correspond to stronger hydrogen bond at the interface. To prove this, we determined the characteristics of the hydrogen bonds at the interface. From the water pair analysis we know that A^I can form hydrogen bonds with various types of water molecules. We also observed that a significant portion of water molecules can interchange between regions A and B (see figure S12). This makes it difficult to distinguish and track individual hydrogen bonds for specific types of water molecules, especially when the tracking time is close to the exchange timescale. Therefore, we investigated hydrogen bond dynamics in the combined A and B regions (AB). For comparison, we also examined hydrogen bond dynamics in regions V, C, and L. The hydrogen-bond (HB) geometry formed between two water molecules is depicted in figure 4(b), with d_{OO} set at 3.2 Å and θ at 30°. We define a correlation function for hydrogen bonds (see SI Formulas for statistical analysis, formula (2)) in a specific region. This correlation function tracks the hydrogen bond over time (in this study, we used 20 ps, figure S11(a)). We then fit the correlation function using two exponential functions (table S3) to obtain the timescales associated with hydrogen bond changes as suggested by previous studies of bulk water molecules [50, 51]. Figure 4(b) displays the slow lifetime of the hydrogen bonds (fast lifetime can be found in table S4). It can be observed that the
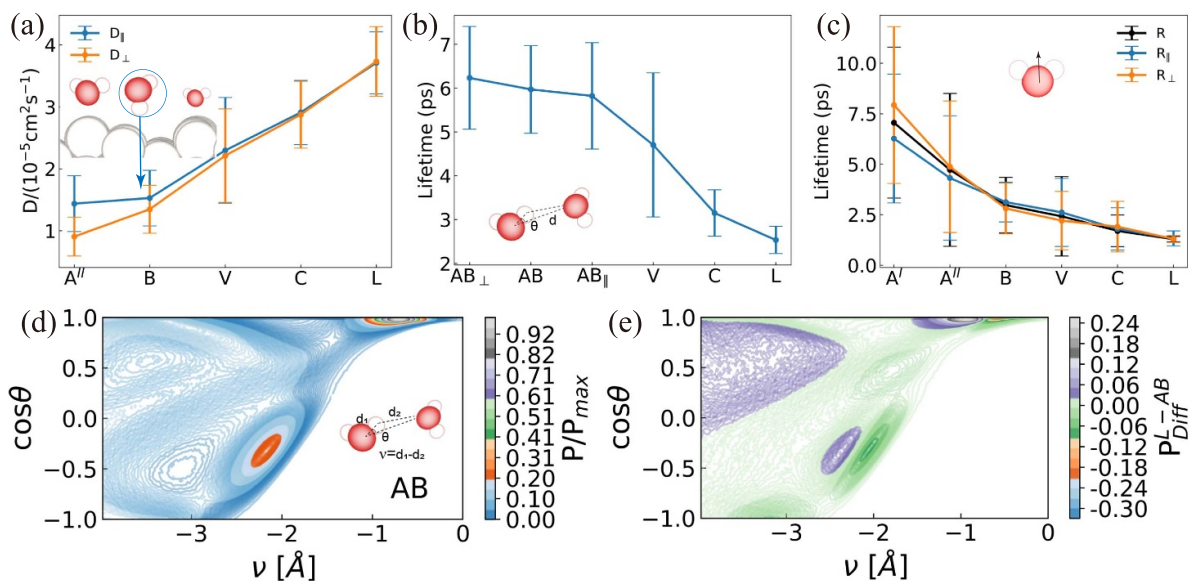
Figure 4. The water dynamics analysis including diffusion/hydrogen bond/reorientation dynamics. (a), The diffusion coefficients of water molecules in different regions. The typical structures of A^I and A^{II} are shown in the inset figure to assist the understanding of anisotropic diffusion dynamics. (b), The hydrogen bond lifetime of the slower part fitted from the hydrogen bond correlation functions using two exponential forms. (c), The reorientation lifetime of the slower part fitted from the second-order rotational autocorrelation functions of the water bisector using two exponential forms. (d), the joint probability distribution of finding an O–H–O$^{'}$ geometry with a given ν–θ configuration for water molecules. Here, ν is the difference between the distance of OH and HO$^{'}$. θ is defined as the angle between OH and OO$^{'}$. For the scale bar, P denotes the frequency count, and Pmax represents the maximum frequency count of a given O–H–O$^{'}$ geometry. P/Pmax denotes the normalized probability distribution. (e), The difference between the normalized hydrogen bond joint probability of water L and AB.

lifetime of the hydrogen bonds will become longer at the interface, in consistent with the observation of slower diffusion dynamics at the interface. We also explored the directionality of hydrogen bond dynamics for water molecules in the AB region. We assessed the directionality of hydrogen bonds at the initial time. Specifically, hydrogen bonds with angles within $-45°-45°$ and $135°-225°$ with respect to the step direction were categorized as parallel to the steps, while the remaining hydrogen bonds were categorized as perpendicular to the step. Our findings indicate that hydrogen bonds perpendicular to the step exhibit greater strength and longer lifetimes compared to those along the step (figure 4(b)). Furthermore, we observed that the percentage of hydrogen bonds perpendicular to the step is higher than those along the step (figure S9), consistent with the observation in figures 2(d)–(i), which shows numerous shorter hydrogen bonds perpendicular to the step. Our previous analysis of water pairs revealed that hydrogen bonds between A^I-A^{II} and A^I-B^I are perpendicular to the step, while those between A^{II}-A^{II} are along the step. This suggests that the anisotropic hydrogen dynamics are primarily influenced by these specific water pairs. It can also be expected that the adsorbed water molecules must rearrange themselves before water dissociation occurs.

To further understand why the diffusion and hydrogen bond dynamics become slower at the interface, we analyzed the joint probability distribution of the O–H–O$^{'}$ geometry (the distance difference ν and the angle θ). Here, ν is defined as the difference between the distance of OH and HO$^{'}$ (in unit of Å). θ is defined as the angle between OH

and OO$^{'}$. The most stable hydrogen bond geometry is located in the top-right corner of figure 4(d) with ν close to -1.0 Å and $\cos\theta$ close to 1.0. Figure 4(e) illustrates the normalized probability difference distribution of hydrogen bond geometry between L and AB. We observed that the hydrogen bond strength at the interface becomes stronger as ν becomes more positive.

The reorientation of water molecules is intricately linked to the dynamic rearrangement and restructuring of the hydrogen bond network [52]. We analyzed the second Legendre polynomials of the correlation function [51] associated with the water bisector, which closely aligns with the direction of the dipole moment (figure S11). During the timescale (20 ps) used to study the reorientation dynamics, different types of water molecules in the B region frequently exchange (figure S12). Therefore, we only analyzed the reorientation dynamics of A^I and A^{II} and treated water molecules in the B region as a whole. Similar to the hydrogen bond dynamics, we used two exponential forms to fit the lifetime, obtaining a slower (figure 4(c)) and a faster (table S3) lifetime. The slower lifetime is presented in the main text. Consistent with the hydrogen bond dynamics, the reorientation dynamics become faster as water molecules move from the interface toward bulk water. We observed that when considering the water bisectors (projected onto the reference plane) of A^I and A^{II}, those with a preference for the direction perpendicular to the step exhibits a longer orientation lifetime, and vice versa. This reorientation dynamics feature aligns with the hydrogen bond directionality of A^I–A^{II} and A^{II}–A^{II} water pairs.

Implications for electrochemistry: one intriguing aspect of interfacial processes is the presence of OH species at Pt sites at low potentials (the H adsorption/desorption region) [17, 53, 54]. This potential region is generally believed to be dominated by H rather than OH [53]. However, recent studies have observed the presence of OH species at low potentials, attributing their formation to water dissociation on stepped Pt sites rather than to oxygenated products formed from the reduction of trace oxygen in the electrolyte [17]. Our simulations suggest that at low potentials, water pairs between $A^I–A^{II}$ and $A^I–B^I$ might serve as crucial resources for water dissociation. The activated chemisorbed water molecules, in conjunction with a physisorbed water molecule, could facilitate OH formation and proton transfer away from the adsorbed OH species. When a third water molecule in the B/V/C region is connected to the prominent water pairs, it will have a higher probability to diffuse and reorient, which may facilitate the proton transfer at the interface.

Aside from the water dissociation, the solvation shell of reactants/ions at the interface may also be modulated by the orientation of the hydrogen bond and then becomes anisotropic at the inner Helmholtz and outer Helmholtz layers. This orientation preference may further affect how the cations/anions play a role in electrochemical reactions.

In conclusion, we have constructed a MLP for the Pt(211)/water interface with first principles accuracy. Using this MLP, we have reproduced the oxygen density profile consistent with AIMD simulations. Importantly, we have identified five distinct types of water molecules and derived three prominent water pairs that may play a significant role in water dissociation. Our analysis reveals that the water diffusion dynamics, hydrogen bond dynamics, and orientation dynamics of both chemisorbed and physisorbed water molecules are anisotropic. They will gradually become isotropic as water molecules approach the bulk region. This suggests that the anisotropic structure and dynamics may play an important role in initiating and facilitating the water dissociation event. The detailed structural and dynamic insights gained from this study also provide a molecular basis for understanding the solvation of reactants and ions at stepped Pt/water interfaces.

4. Future perspectives

This paper mainly studied the *in situ* structure and dynamics at stepped Pt/water interface and established connection between the structure and dynamics. With the rapid development of MLP method, the study of *in situ* structure and dynamics at metal/water interfaces will be a conventional method. Nevertheless, the deconvolution of the complex and hierarchical dynamics at the interfaces is still a grand challenge. For example, the water adlayer evolution at the metal/water interfaces were reported to happen at the timescale from several hundred picoseconds to several nanoseconds, which needs further examination. In addition, the study of charged metal/water interfaces calls for the establishment of solid method to incorporate the long range interactions. For example, the cations effect has recently attracted many attentions due to its special

role in tuning the reactivity and selectivity of many electrochemical reactions. What are the main feature of the hydration structures of the ions and how do ions distribute at the interfaces are some fundamental issues that need to be addressed to gain deep insights into the electrochemical reactions at molecular level.

Data availability

The machine learning potential model and the Pt(211)/water interface model are available at https://dataverse.ikkem.com/dataverse.xhtml.

Acknowledgments

Author contributions

F T W and X L and J C designed research; F T W performed research; F T W and X L and J C analyzed data; F T W X L and J C wrote the paper.

Conflict of interest

The authors declare no conflict of interest.

ORCID iD

Jun Cheng https://orcid.org/0000-0001-6971-0797

References

[1] Björneholm O *et al* 2016 Water at interfaces *Chem. Rev.* **116** 7698–726

[2] Marini L 2010 Thermodynamics and kinetics of water–rock interaction *Geofluids* **10** 452–4

[3] Peng J, Guo J, Ma R and Jiang Y 2022 Water-solid interfaces probed by high-resolution atomic force microscopy *Surf. Sci. Rep.* **77** 100549

[4] Taylor C D 2012 Atomistic modeling of corrosion events at the interface between a metal and its environment *Int. J. Corros.* **2012** 1–13

[5] Su M, Dong J-C and Li J-F 2020 In-situ Raman spectroscopic study of electrochemical reactions at single crystal surfaces *J. Electrochem.* **26** 54–60

[6] van der Niet M J, den Dunnen A, Juurlink L B and Koper M T 2010 The influence of step geometry on the desorption characteristics of O2, D2 and H2O from stepped Pt surfaces *J. Chem. Phys.* **132** 174705

[7] Schouten K J, van der Niet M J and Koper M T 2010 Impedance spectroscopy of H and OH adsorption on

stepped single-crystal platinum electrodes in alkaline and acidic media *Phys. Chem. Chem. Phys.* **12** 15217–24

[8] Creighan S C, Mukerji R J, Bolina A S, Lewis D W and Brown W A 2003 The adsorption of CO on the stepped Pt211 surface: a comparison of theory and experiment *Catal. Lett.* **88** 39–45

[9] Liu G, Shih A J, Deng H, Ojha K, Chen X, Luo M, McCrum I T, Koper M T M, Greeley J and Zeng Z 2024 Site-specific reactivity of stepped Pt surfaces driven by stress release *Nature* **626** 1005–10

[10] Limmer D T, Willard A P, Madden P and Chandler D 2013 Hydration of metal surfaces can be dynamically heterogeneous and hydrophobic *Proc. Natl Acad. Sci. USA* **110** 4200–5

[11] Zhu J-X, Le J-B, Koper M T M, Doblhoff-Dier K and Cheng J 2021 Effects of adsorbed OH on Pt(100)/water interfacial structures and potential *J. Phys. Chem.* C **125** 21571–9

[12] Waegele M M, Gunathunge C M, Li J and Li X 2019 How cations affect the electric double layer and the rates and selectivity of electrocatalytic processes *J. Chem. Phys.* **151** 160902

[13] Zwaschka G, Lapointe F, Campen R K and Tong Y 2021 Characterization of ultrafast processes at metal/solution interfaces: towards femtoelectrochemistry *Curr. Opin. Electrochem.* **29** 100813

[14] Rizo R, Herrero E, Climent V and Feliu J M 2023 On the nature of adsorbed species on platinum single-crystal electrodes *Curr. Opin. Electrochem.* **38**

[15] Li J-L, Li Y-F and Liu Z-P 2022 Recent advances in electrochemical kinetics simulations and their applications in pt-based fuel cells *J. Electrochem.* **28** 2108511

[16] Chinese Society of Electrochemistry 2024 The top ten scientific questions in electrochemistry *J. Electrochem.* **30** 2024121

[17] Rizo R, Fernandez-Vidal J, Hardwick L J, Attard G A, Vidal-Iglesias F J, Climent V, Herrero E and Feliu J M 2022 Investigating the presence of adsorbed species on Pt steps at low potentials *Nat. Commun.* **13** 2550

[18] Kolb M J, Wermink J, Calle-Vallejo F, Juurlink L B and Koper M T 2016 Initial stages of water solvation of stepped platinum surfaces *Phys. Chem. Chem. Phys.* **18** 3416–22

[19] Bu Y, Cui T, Zhao M, Zheng W, Gao W and Jiang Q 2018 Evolution of water structures on stepped platinum surfaces *J. Phys. Chem.* C **122** 604–11

[20] Gross A, Gossenberger F, Lin X H, Naderian M, Sakong S and Roman T 2014 Water structures at metal electrodes studied by ab initio molecular dynamics simulations *J. Electrochem. Soc.* **161** E3015–20

[21] Grecea M L, Backus E H G, Riedmüller B, Eichler A, Kleyn A W and Bonn M 2004 The interaction of water with the Pt(533) surface *J. Phys. Chem.* B **108** 12575–82

[22] Endo O, Nakamura M, Sumii R and Amemiya K 2012 1D hydrogen bond chain on Pt(211) stepped surface observed by O K-NEXAFS spectroscopy *J. Phys. Chem.* C **116** 13980–4

[23] Kolb M J, Farber R G, Derouin J, Badan C, Calle-Vallejo F, Juurlink L B, Killelea D R and Koper M T 2016 Double-stranded water on stepped platinum surfaces *Phys. Rev. Lett.* **116** 136101

[24] Mistry K, Gerrard N and Hodgson A 2023 Wetting of a stepped platinum (211) surface *J. Phys. Chem.* C **127** 4741–8

[25] Carrasco J, Hodgson A and Michaelides A 2012 A molecular perspective of water at metal interfaces *Nat. Mater.* **11** 667–74

[26] Rizo R, Sitta E, Herrero E, Climent V and Feliu J M 2015 Towards the understanding of the interfacial pH scale at Pt(1 1 1) electrodes *Electrochim. Acta* **162** 138–45

[27] Zhong G *et al* 2022 Determining the hydronium pK[Formula: see text] at platinum surfaces and the effect on pH-dependent hydrogen evolution reaction kinetics *Proc. Natl Acad. Sci. USA* **119** e2208187119

[28] Nakamura M, Sato N, Hoshi N, Soon J M and Sakata O 2009 One-dimensional zigzag chain of water formed on a stepped surface *J. Phys. Chem.* C **113** 4538–42

[29] Toney M F, Howard J N, Richer J, Borges G L, Gordon J G, Melroy O R, Wiesler D G, Yee D and Sorensen L B 1994 Voltage-dependent ordering of water molecules at an electrode-electrolyte interface *Nature* **368** 444–6

[30] Velasco-Velez J J, Wu C H, Pascal T A, Wan L F, Guo J, Prendergast D and Salmeron M 2014 The structure of interfacial water on gold electrodes studied by x-ray absorption spectroscopy *Science* **346** 831–4

[31] Li C Y, Le J B, Wang Y H, Chen S, Yang Z L, Li J F, Cheng J and Tian Z Q 2019 In situ probing electrified interfacial water structures at atomically flat surfaces *Nat. Mater.* **18** 697–701

[32] Chen W, Yu A, Sun Z-J, Zhu B-Q, Cai J and Chen Y-X 2019 Probing complex eletrocatalytic reactions using electrochemical infrared spectroscopy *Curr. Opin. Electrochem.* **14** 113–23

[33] Geissler P L, Dellago C, Chandler D, Hutter J and Parrinello M 2001 Autoionization in liquid water *Science* **291** 2121–4

[34] Hassanali A, Prakash M K, Eshet H and Parrinello M 2011 On the recombination of hydronium and hydroxide ions in water *Proc. Natl Acad. Sci. USA* **108** 20410–5

[35] Groß A and Sakong S 2022 Ab initio simulations of water/metal interfaces *Chem. Rev.* **122** 10746–76

[36] VandeVondele J, Krack M, Mohamed F, Parrinello M, Chassaing T and Hutter J 2005 Quickstep: fast and accurate density functional calculations using a mixed Gaussian and plane waves approach *Comput. Phys. Commun.* **167** 103–28

[37] Goedecker S, Teter M and Hutter J 1996 Separable dual-space Gaussian pseudopotentials *Phys. Rev.* B **54** 1703–10

[38] Hartwigsen C, Goedecker S and Hutter J 1998 Relativistic separable dual-space Gaussian pseudopotentials from H to Rn *Phys. Rev.* B **58** 3641–62

[39] VandeVondele J and Hutter J 2007 Gaussian basis sets for accurate calculations on molecular systems in gas and condensed phases *J. Chem. Phys.* **127** 114105

[40] Le J, Iannuzzi M, Cuesta A and Cheng J 2017 Determining potentials of zero charge of metal electrodes versus the standard hydrogen electrode from density-functional-theory-based molecular dynamics *Phys. Rev. Lett.* **119** 016801

[41] Perdew J P, Burke K and Ernzerhof M 1996 Generalized gradient approximation made simple *Phys. Rev. Lett.* **77** 3865–8

[42] Grimme S, Antony J, Ehrlich S and Krieg H 2010 A consistent and accurate ab initio parametrization of density functional dispersion correction (DFT-D) for the 94 elements H-Pu *J. Chem. Phys.* **132** 154104

[43] Zhang Y, Wang H, Chen W, Zeng J, Zhang L, Wang H and Weinan E 2020 DP-GEN: a concurrent learning platform for the generation of reliable deep learning based potential energy models *Comput. Phys. Commun.* **253** 107206

[44] Zhang L, Han J, Wang H, Car R and Weinan E 2018 Deep potential molecular dynamics: a scalable model with the accuracy of quantum mechanics *Phys. Rev. Lett.* **120** 143001

[45] Plimpton S 1995 Fast parallel algorithms for short-range molecular-dynamics *J. Comput. Phys.* **117** 1–19

[46] Nosé S 1984 A unified formulation of the constant temperature molecular dynamics methods *J. Chem. Phys.* **81** 511–9

[47] Hoover W G 1985 Canonical dynamics: equilibrium phase-space distributions *Phys. Rev.* A **31** 1695–7

[48] Chen A, Le J-B, Kuang Y and Cheng J 2022 Modeling stepped Pt/water interfaces at potential of zero charge with ab initio molecular dynamics *J. Chem. Phys.* **157** 094702

[49] Le J, Cuesta A and Cheng J 2018 The structure of metal-water interface at the potential of zero charge from density functional theory-based molecular dynamics *J. Electroanal. Chem.* **819** 87–94

[50] Liu J, He X, Zhang J Z H and Qi L W 2018 Hydrogen-bond structure dynamics in bulk water: insights from ab initio simulations with coupled cluster theory *Chem. Sci.* **9** 2065–73

[51] Woutersen S, Emmerichs U and Bakker H J 1997 Femtosecond mid-IR pump-probe spectroscopy of liquid water: evidence for a two-component structure *Science* **278** 658–60

[52] Laage D and Hynes J T 2006 A molecular jump mechanism of water reorientation *Science* **311** 832–5

[53] Kolb M J, Calle-Vallejo F, Juurlink L B and Koper M T 2014 Density functional theory study of adsorption of H_2O, and H_2O stepped platinum surfaces *J. Chem. Phys.* **140** 134708

[54] Attard G A, Hunter K, Wright E, Sharman J, Martínez-Hincapié R and Feliu J M 2017 The voltammetry of surfaces vicinal to Pt110: structural complexity simplified by CO cooling *J. Electroanal. Chem.* **793** 137–46